2009 American Control Conference
Hyatt Regency Riverfront, St. Louis, MO, USA
June 10-12, 2009

Improved noise sensitivity under high-gain feedback in nano-positioning motion systems

Marcel Heertjes, George Leenknegt, Bram van Goch, and Henk Nijmeijer

Abstract— **To avoid an increased noise response under high-gain feedback in nano-positioning motion systems, a nonlinear (N-PID) control design is proposed. The design is of particular interest in the wafer scanning industry where nano-accuracy should be achieved under high-speed motion. In a variable gain controller setting, the N-PID control design has an observer structure with state-dependent low-pass filter characteristics. Under high-gain feedback and being induced by sufficiently large servo error signals, the nonlinear observer acts as a low-pass filter with a significantly smaller cut-off frequency as compared to the case of low-gain feedback. As a result, the high-frequency noise response that usually increases under high-gain feedback is kept limited. For a validated wafer stage model, the effectiveness of the control approach in dealing with position-dependent behavior is assessed through simulation.**

I. Introduction

In many motion control systems, performance is key to the success of the control design. Examples of such systems include the fast and nano-scale motion control of the stages in wafer scanners which are used in the manufacturing of integrated circuits, the positioning systems of storage drives like compact disk, digital versatile disk, blu-ray disk, and hard-disk drives, and the scanning stages of electron microscopes used for sub-micron imaging; see [1], [2], [3].

Servo performance is often expressed in terms of disturbance rejection and noise sensitivity. In fact, most controllers aim at improved low-frequency disturbance suppression while maintaining favorable high-frequency noise properties. Bound by inherent design limitations, however, linear feedback design generally fails in satisfying this aim to the fullest. Different from linear control, nonlinear control then adds more freedom in the control design which can be attended toward the direction of improved performance. For example in the process of wafer scanning, disturbances and related servo signals may differ significantly from one location on the wafer to another. As such, a high-gain controller may perform favorably on one location but is outperformed by a low-gain controller at another location. This hints toward varying the controller gains as a means to exceed beyond the possibilities given by the nominal (and linear) control design.

In N-PID control, see also [4], [5], [6], the controller gain is adapted according to the (estimated) servo signals at hand. This generally gives more flexibility in dealing with position-dependent disturbances but the problem of noise amplification under high-gain feedback remains. To cope with this problem we study a nonlinear observer whose cut-off frequency is lowered under increased gains. This counteracts a potential increase in noise response, hence the kind of high-frequency response that would typically occur in the observer's absence while operating under high-gain feedback, but largely preserves the high-gain disturbance rejection properties. Different from [7], [8], [9], [10], [11] or [12] (the latter using variable gains) where observer-based control designs are described that keep the underlying stability result (through the circle criterion) valid, the focus of the design described here is on achieving performance. In so doing, the linear part of the observer design is brought down to its basic form: a first-order low-pass filter. The control design is tested through simulation using a validated model of a wafer stage derived from an industrial wafer scanner. It shows the ability to improve upon low-frequency disturbance rejection properties in certain parts of the scan while maintaining a small high-frequency noise response in other parts.

This paper is further organized as follows. In Section II, the variable gain control design is presented within the considered class of motion control systems. In Section III, a design for stability is presented which aims at robust stability under conditions of improved low-frequency disturbance rejection. In terms of performance, Section IV provides tuning rules regarding the observer parameters. Also, the effectiveness of the design in achieving improved low-frequency disturbance rejection while maintaining a small high-frequency noise response is assessed in simulation on a validated model of a wafer stage. The paper is concluded in Section V.

II. N-PID Control Design

To improve upon the low-frequency disturbance rejection properties of motion systems, variable gain control embedded in a nominal PID-controller structure (see also [13]) is used in optical storage drives, vibrations isolation systems, and wafer scanner. For these systems, the simplified feedback scheme of Fig.1 often suffices to represent the nominal (and linear) control design. That is, a single-input single-output

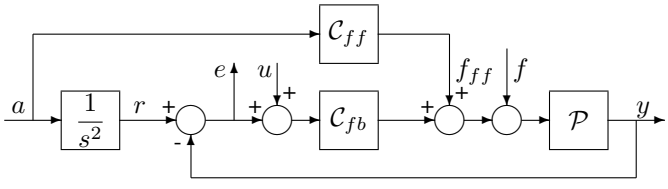

Fig. 1. Single-input single-output motion control scheme.

(SISO) feedback controller $\mathcal{C}_{fb}$ and a SISO feed forward controller $\mathcal{C}_{ff}$ are used to control the strictly proper plant

$\mathcal{P}$. The output y along with a reference command (or set-point) r forms the controller error e via $e = r - y$.

Key to the design is the introduction of a nonlinear controller gain which in view of the incidental, often non-stationary, and position-dependent expression of disturbances f adapts the disturbance rejection properties of the feedback design according to the disturbances at hand. Hereto the error e (see Fig.1) is fed into an extra and generally nonlinear controller, which consists of a nonlinear and a linear part. The nonlinear part is given in time-domain by

$$e_\phi(t) = \phi(e(t))e(t), \tag{1a}$$

with $\phi(\cdot)$ a nonlinear gain operation satisfying $0 \leq \phi(\cdot) \leq \alpha$ with $\alpha > 0$. The linear part is given in the Laplace-domain by

$$\frac{u(s)}{e_\phi(s)} = \mathcal{F}_1(s), \tag{1b}$$

with $\mathcal{F}_1$ a loop shaping filter and u representing the output of the nonlinear connection, see also [14].

A major benefit from incorporating a nonlinear feedback is that sporadically significant improvements in low-frequency disturbance rejection can be obtained (when necessary from a performance perspective) for a proper choice of $\mathcal{F}_1$ and ϕ. Namely for the considered class of systems in Fig.1 and given $\phi = \alpha > 0$ (this is referred to as the linear high-gain limit) the sensitivity function between e and r, which expresses the ability to keep the low-frequency servo errors small in view of input disturbances, is given by

$$\lim_{\omega\to 0}\left\{\frac{e(j\omega)}{r(j\omega)}\right\}_{hg} = \frac{1}{(1+\alpha\mathcal{F}_1(j\omega))\mathcal{C}_{fb}(j\omega)\mathcal{P}(j\omega)}, \tag{2}$$

thus giving a factor of $1 + \alpha\mathcal{F}_1$ extra low-frequency disturbance rejection when compared to the case of $\phi = \alpha = 0$, hence in absence of the nonlinear feedback. This low-frequency improvement, however, comes at the cost of an increased sensitivity to high-frequency noises. This follows from the high-gain complementary sensitivity function between y and r which expresses the ability to limit the high-frequency output in view of output noises, and which is given by

$$\lim_{\omega\to\infty}\left\{\frac{y(j\omega)}{r(j\omega)}\right\}_{hg} \approx (1+\alpha\mathcal{F}_1(j\omega))\mathcal{C}_{fb}(j\omega)\mathcal{P}(j\omega). \tag{3}$$

So increased low-frequency disturbance rejection under high-gain feedback (see (2) by a factor of $1 + \alpha\mathcal{F}_1$) corresponds to an increased noise sensitivity by the same amount (see (3)). It is the aim of this paper to (ultimately) avoid such a trade-off.

Hereto a combined nonlinear observer/controller structure is proposed such as depicted in Fig.2. Key to the observer is the fact that apart from its linear low-pass filter characteristics reflected by $\mathcal{F}_2$, the nonlinear controller output u is used in the observed error $\hat{e}$. As a result, a nonlinear observer is obtained that satisfies the following relations

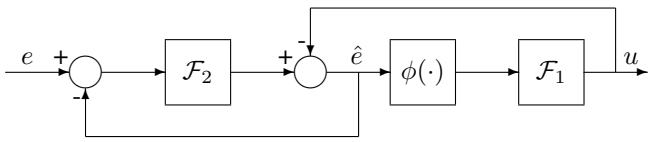

Fig. 2. Variable gain observer/controller scheme.

$$\begin{aligned}\mathcal{L}\{\hat{e}(t)\} &= \mathcal{F}_2(s)\mathcal{L}\{e(t)-\hat{e}(t)\} - \mathcal{L}\{u(t)\}\\ &= \mathcal{F}_2(s)\mathcal{L}\{e(t)-\hat{e}(t)\} - \mathcal{F}_1(s)\mathcal{L}\{\hat{e}_\phi(t)\},\end{aligned} \tag{4}$$

with $\hat{e}_\phi(t) = \phi(\hat{e}(t))\hat{e}(t)$. The observer characteristics can be partly assessed through the following linear limits

$$\lim_{\phi(\hat{e}(t))\to 0}\left\{\frac{\hat{e}(j\omega)}{e(j\omega)}\right\}_{lg} = \frac{\mathcal{F}_2(j\omega)}{1+\mathcal{F}_2(j\omega)}, \tag{5a}$$

and

$$\lim_{\phi(\hat{e}(t))\to \alpha}\left\{\frac{\hat{e}(j\omega)}{e(j\omega)}\right\}_{hg} = \frac{\mathcal{F}_2(j\omega)}{1+\mathcal{F}_2(j\omega)+\alpha\mathcal{F}_1(j\omega)}. \tag{5b}$$

For small error levels and if $\omega \to \infty$, the observer tends to the low-gain characteristics determined by $\mathcal{F}_2$, see (5a). Contrarily for sufficiently large error levels, the observer tends to the high-gain characteristics $\mathcal{F}_2(1 + \alpha\mathcal{F}_1)^{-1}$, see (5b). It is assumed that $\mathcal{F}_2$ has low-pass characteristics whereas $\mathcal{F}_1$ does not. As a result the increased high-frequency noise sensitivity by a factor of $1 + \alpha\mathcal{F}_1$ under high-gain feedback, see (3), is fully counteracted by the observer.

Given the nonlinear observer in Fig.2, its choice of filters and the parameters therein reflects two different design approaches. Filter $\mathcal{F}_1$ is mainly designed in the context of closed-loop stability (Section III) whereas filter $\mathcal{F}_2$ and ϕ are designed in view of closed-loop performance (Section IV).

III. Design for Stability

Design for stability mainly refers to the choice of $\mathcal{F}_1$ in view of closed-loop stability. Apart from guaranteeing stability using results from absolute stability theory, in particular the circle criterion, this circle criterion is also used to design a loop shaping filter $\mathcal{F}_1$; see also [12], [10] with a similar aim. The latter is needed to support a gain increase for improved low-frequency disturbance rejection, see also [14]. For this purpose, we adopt the absolute stability representation of Fig.3 where $\mathcal{G}(j\omega) = \mathcal{C}_{fb}(j\omega)\mathcal{P}(j\omega)/(1 + \mathcal{C}_{fb}(j\omega)\mathcal{P}(j\omega))$ and $\Phi(e_{12}, t) = (\phi(e_1)e_1 - \phi(e_2)e_2)/e_{12}$ with $e_{12} = e_1 - e_2$ and for which we define $e_1 = e_2 \to \Phi(e_{12}, t) := 0$. Closed-loop stability is guaranteed on the basis of the next result.

Theorem 3.1: Assume the system $\mathcal{P}$ in Fig.1 is globally asymptotically stabilized by $\mathcal{C}_{fb}$. Moreover, assume $\mathcal{F}_1$, $\mathcal{F}_2$ and $1/(1 + \mathcal{F}_2)$ Hurwitz. Then any observer of the form as considered in Fig.2 with $0 \leq \Phi(\cdot, t), \phi(\cdot) \leq \alpha$ globally asymptotically stabilizes $\mathcal{P}$ if

$$\Re\left\{\frac{\mathcal{F}_1(j\omega)\mathcal{F}_2(j\omega)\mathcal{G}(j\omega) - \mathcal{F}_1(j\omega)}{1+\mathcal{F}_2(j\omega)}\right\} \geq -\frac{1}{\alpha}. \tag{6}$$

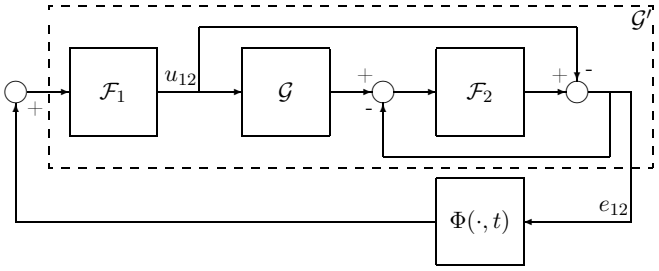

Fig. 3. Incremental nonlinear dynamics in Lur'e form with observer.

Proof: If $\mathcal{C}_{fb}$ globally asymptotically stabilizes $\mathcal{P}$, then the closed-loop transfer $\mathcal{G}(j\omega)$ is Hurwitz. Furthermore, from the feedback connection of Fig.3, a frequency response function $\mathcal{G}'(j\omega)$ follows that reads

$$\mathcal{G}'(j\omega) = \frac{\mathcal{F}_1(j\omega)}{1+\mathcal{F}_2(j\omega)}\left\{\mathcal{F}_2(j\omega)\mathcal{G}(j\omega) - 1\right\}. \qquad (7)$$

The first part of this transfer is Hurwitz. The second part is also Hurwitz because the poles of $\mathcal{F}_2(s)\mathcal{G}(s) - 1$ are determined by the poles of $\mathcal{F}_2(s)\mathcal{G}(s)$. As a result $\mathcal{G}'(j\omega)$ is Hurwitz which combined with the fact that $\Phi(\cdot,t)$ (and $\phi(\cdot)$) satisfies the sector condition $0 \leq \Phi(\cdot,t) \leq \alpha$ allows for proving absolute stability through the circle criterion, see, for example, [15]. ■

Example 3.1: To illustrate the value of the result in (6), a scanning wafer stage is used as a benchmark example, see Fig.4. In such systems, light from a laser that is passing through a mask and scaled by a lens is projected onto a wafer. The wafer is located atop a wafer stage which represents a

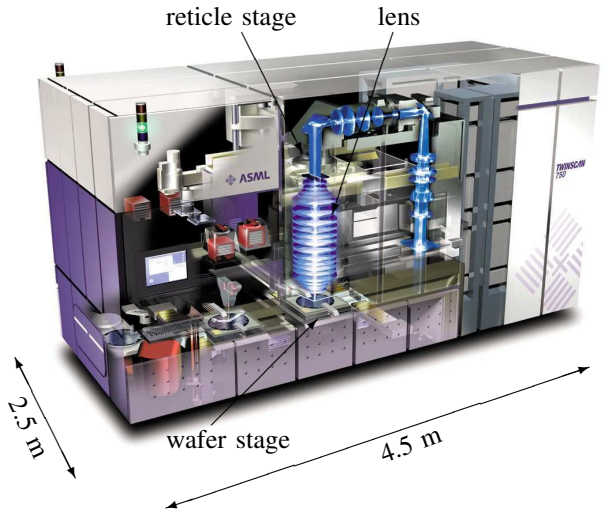

Fig. 4. Artist impression of an industrial wafer scanner.

floating mass that is controlled in six degrees-of-freedom. For the vertical z-direction (see also [14]), a simplified wafer stage plant model is given by

$$\mathcal{P}(s) = \frac{7s^2 + 90s + 9.2\ 10^7}{108.5s^4 + 2025s^3 + 2.07\ 10^9 s^2}. \qquad (8)$$

The corresponding feedback controller reads

$$\mathcal{C}_{fb}(s) = \mathcal{F}_{pid}(s)\mathcal{F}_{lp}(s)\mathcal{F}_n(s), \qquad (9)$$

with

$$\mathcal{F}_{pid}(s) = \frac{8.1\ 10^6\left(s^2 + 776s + 1.5\ 10^5\right)}{415s}, \qquad (10)$$

$$\mathcal{F}_{lp}(s) = \frac{1.2\ 10^7}{s^2 + 398s + 1.2\ 10^7}, \qquad (11)$$

and

$$\mathcal{F}_n(s) = \frac{0.6s^6 + 1773s^5 + 4.3\ 10^7 s^4 + 4.4\ 10^{10}s^3}{s^6 + 10^4 s^5 + 6.2\ 10^7 s^4 + 2.3\ 10^{11}s^3} \cdots \qquad (12)$$

$$\frac{6.3\ 10^{14}s^2 + 1.4\ 10^{17}s + 5\ 10^{19}}{5.6\ 10^{14}s^2 + 3.7\ 10^{16}s + 5\ 10^{19}}. \qquad (13)$$

In the implementation a discrete-time version of this controller is used on the basis of a sampling frequency of 5 kHz. By means of example, the filters $\mathcal{F}_1$ and $\mathcal{F}_2$ in the nonlinear observer structure of Fig.2 are given by

$$\mathcal{F}_1(s) = \frac{2.5\ 10^7 s^2 + 4.2\ 10^{10}s + 4.9\ 10^{13}}{s^4 + 2\ 10^4 s^3 + 1.2\ 10^8 s^2 + 3.5\ 10^{11}s + 4.9\ 10^{13}}, \qquad (14)$$

and

$$\mathcal{F}_2(s) = \frac{3574}{s + 1131}. \qquad (15)$$

For this controlled wafer stage model, the graphical interpretation of (6) is shown in Fig.5 by plotting the corresponding frequency response functions: measured (solid) and simulated (dashed). The main cause for deviation between both relates to the differences between discrete-time implementation and continuous-time simulation. For the case that

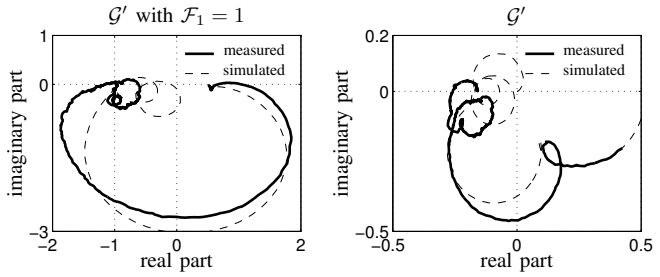

Fig. 5. Graphical interpretation of (6) without loop shaping filter $\mathcal{F}_1$ (left) and with loop shaping filter $\mathcal{F}_1$ (right).

$\mathcal{F}_1 = 1$ (this is the left part of the figure) it follows that stability using the circle criterion is sufficiently guaranteed if the frequency response function $\mathcal{G}'$ remains to the right of a vertical line through the point (-1.9,0). As a result, stability through the circle criterion is guaranteed for extra gains up to $\alpha = 1/1.9 \approx 0.5$. The extra gains are limited by the fact that $\lim_{\omega\to\infty} \mathcal{G}'(j\omega) \to -1$. By definition α cannot exceed the value of $\alpha = 1$. To avoid this limitation and hence the potential increase of extra gain α, the loop shaping filter $\mathcal{F}_1$ is chosen strictly proper, see (14). The effect is shown in the right part of the figure. Here $\mathcal{G}'$ remains to the right of a vertical line through the point (-0.28,0) such that α can be chosen up to $\alpha = 1/0.28 \approx 3.6$. The need to choose

$\mathcal{F}_1$ strictly proper potentially conflicts with the desired high-gain observer limit in (5). For sufficiently large error levels, the high-gain observer limit now tends to the low-gain observer limit. As a result, the increased high-frequency noise sensitivity by a factor of $1 + \alpha\mathcal{F}_1$ under high-gain feedback in (3) is no longer counteracted by the observer. In a discrete-time control setting, however, the cut-off frequencies in $\mathcal{F}_1$ and $\mathcal{F}_2$ can be tuned sufficiently discriminative as to simultaneously access large extra gain values and still counteract significant parts of the increased noise response. This is shown in Fig.6 through the frequency response from e to $\hat{e}$ and in terms of the linear observer limits, see also (5). Apart from the first-order low-pass characteristics, it

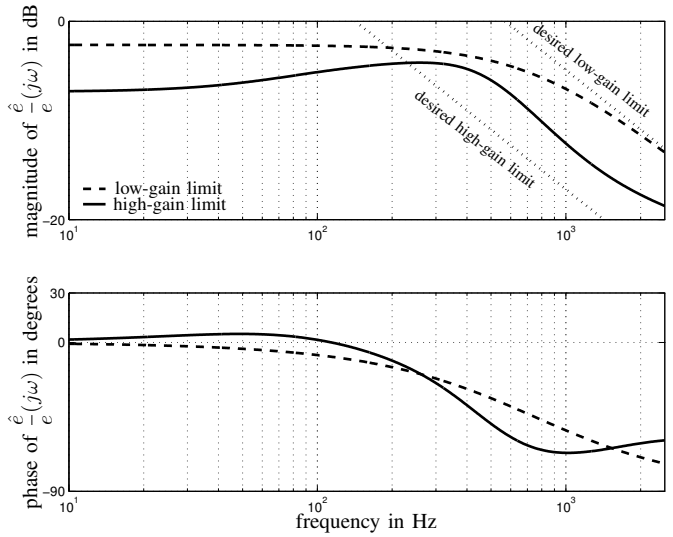

Fig. 6. Bode representation of the observer frequency response function limits in (5): the low-gain limit (dashed) and the high-gain limit (solid).

can be seen that the high-gain observer limit gives access to extra high-frequency reduction. This reduction provides a means to compensate for the increased high-frequency noise amplification induced by $\mathcal{G}$ under high-gain feedback. Note that for $\alpha = 3$ a reduction of $(1 + \alpha)^{-1} \rightarrow 12$ dB is not reached; see the pair of dashed lines indicating the desired low-pass characteristics. This is because $\mathcal{F}_1$ includes a low-pass filter (see (14)) such that both the high- and low-gain observer limits ultimately converge. The current choice for $\mathcal{F}_1$, however, gives extra broad-band noise suppression below the Nyquist frequency of the discrete-time control design. Apart from extra noise suppression, the high-gain observer limit in Fig.6 shows deteriorated low-frequency properties.

IV. Design for Performance

Design for performance refers to the choice for the nonlinearity ϕ and the observer $\mathcal{F}_2$. For ϕ, the distinction between stability and performance is evident. Namely given the class of sector-bounded nonlinearities $0 \leq \phi(\cdot) \leq \alpha$, the choice for ϕ is invariant under the stability result in (6) but it does affect the servo performance related to it. For the filter design of $\mathcal{F}_2$ (and also $\mathcal{F}_1$) such a distinction is less apparent. Nevertheless $\mathcal{F}_2$ is primarily designed in view of closed-loop servo performance.

In designing the nonlinearity, ϕ is given the following dead-zone characteristics

$$\phi(\hat{e}(t)) = \begin{cases} 0, \text{ if } |\hat{e}(t)| \leq \delta, \\ \alpha - \dfrac{\alpha\delta}{|\hat{e}(t)|}, \text{ if } |\hat{e}(t)| > \delta, \end{cases} \tag{16}$$

with α a gain and δ a switching length. It can be verified that (16) satisfies the imposed conditions on stability in (6), *i.e.*, $0 \leq \phi(\hat{e}(t)) \leq \alpha$ and $0 \leq \Phi(\hat{e}_{12}, t) \leq \alpha$. The idea of using a dead-zone filter operation is motivated as follows. For large-amplitude (and sporadically occurring) error signals $\hat{e}$, which apply to the frequency range below the controller bandwidth, it is assumed that the switching length δ is sufficiently exceeded. This induces extra gain which incidentally gives rise to extra disturbance suppression. Contrarily for small-amplitude noise occurring during steady-state operation, the switching length is not exceeded. So no extra gain is induced, thus maintaining a low-gain noise response.

In tuning the filter parameters in ϕ, the value for α follows from the loop-shaping argument considered in Example 3.1 from which α is given the sufficiently robust value of $\alpha = 3$. Tuning δ is related to the discrimination between signal and noise during the wafer scanning interval which follows from a more ad hoc argument where the smallest upper bound on the servo error signals during (constant velocity) scanning is used as an initial estimate, or

$$\delta = \lim_{t \rightarrow \infty} \sup |e(t)|, \tag{17}$$

and which is (possibly) fine tuned during the process of achieving servo performance. This is shown in Fig.7 where

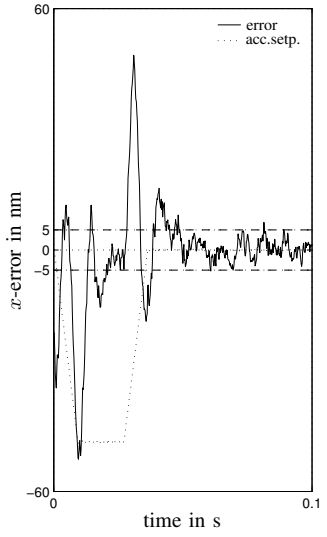

Fig. 7. Time-series measurement of the servo error signals at die five in relation with the tuned parameter setting of $\delta = 5$ nm.

it can be seen that during scanning the maximum absolute value of the measured error signal in x-direction roughly remains below the switching length of $\delta = 5$ nm. This

keeps a potential noise amplification during scanning limited whereas performance limiting oscillations related to the acceleration set-point (dotted curve denoted with acc.setp.) prior to the scan induce extra controller gain, thus extra disturbance suppression.

In designing the linear observer part $\mathcal{F}_2$, it is natural to adopt the structure of system $\mathcal{G}$ which is generally a high-order complementary sensitivity function. To limit the observer order, however, which generally makes the design more attractive from an implementation point of view, $\mathcal{G}$ is approximated by a single first-order low-pass filter:

$$\mathcal{F}_2(s) = \frac{\gamma\ \omega_{\rm lp}}{s+\ \omega_{\rm lp}}, \tag{18}$$

with γ a tuning parameter and $\omega_{\rm lp}$ the cut-off frequency which is chosen near the (low-gain) controller bandwidth; see also (15). The tuning parameter γ determines the low-frequency magnitude in the transfer from measured error e to observed error $\hat{e}$, see also Fig.2. So γ is part of a performance trade-off. Choosing γ small results in limited (extra) low-frequency disturbance rejection. Choosing γ large results in a high observer's cut-off frequency giving an increased noise response. For the considered wafer stage example $\gamma = 3.16$.

Example 4.1: Given the nonlinear observer, wafer stage performance is assessed (through simulation) at five distinct locations on the wafer. These locations are shown in Fig.8 and are labelled with die one through die five. Apart from

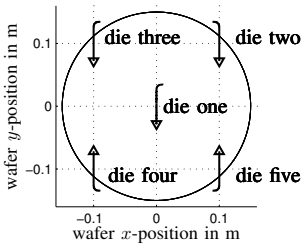

Fig. 8. Schematic overview of five different scan locations along the wafer.

the sign, at each die a comparable scan is performed in terms of x- and y-acceleration set-points. The corresponding servo errors are depicted in Fig.9. Herein two filter operations are adopted from the semiconductor industry: the moving average filter operation and the moving standard deviation filter operation. The moving average operation, or

$$\mathcal{M}_{\rm a}(i) = \frac{1}{n}\sum_{j=i-n/2}^{i+n/2-1} e(j),\ \forall i \in \mathbb{Z}, \tag{19}$$

with n a scanning time-scale parameter, essentially is a low-pass filter operation on the discrete-time error $e(i)$, which is used to express the ability to position a single exposed wafer layer atop another; so-called scanning overlay [16]. The moving standard deviation filter operation, or

$$\mathcal{M}_{\rm sd}(i) = \frac{1}{n}\sum_{j=i-n/2}^{i+n/2-1} \sqrt{(e(j)-\mathcal{M}_{\rm a}(i))^2},\ \forall i \in \mathbb{Z}, \tag{20}$$

is a high-pass filter which is used to express the deviation

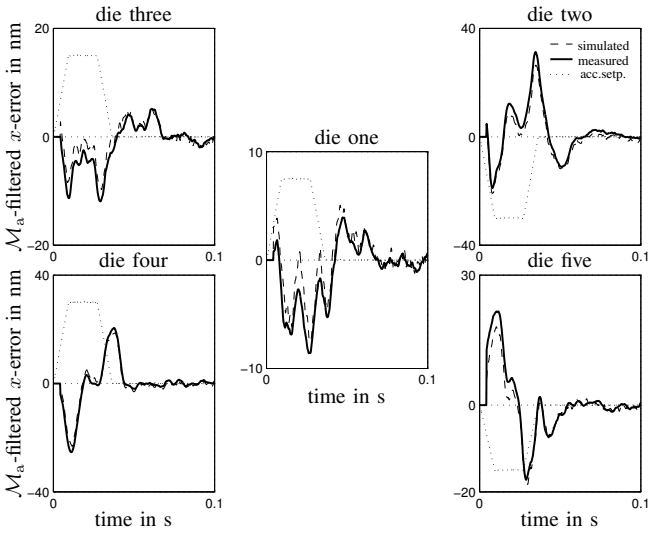

Fig. 9. Time-series simulation versus measurement along the wafer.

in equal positioning tasks; so-called fading. In Fig.9, simulations are based on a finite element model of the wafer stage plant capturing the dynamics at the five considered die locations. The model gives rise to position-dependent servo error behavior which can be best seen when comparing the error responses from die one with die three, both of which are the result of the same (scaled) acceleration set-points but applied at different locations. The figure also contains time-series measurements obtained from an industrial (scanning) wafer stage. It is concluded that a fairly good comparison is obtained between simulation and measurement.

Having this validated model, the effect of the nonlinear observer can be assessed through simulation. In terms of moving average filtered error responses, Fig.10 shows the effect of the low-gain linear control design with $\alpha = 0$, the high-gain linear control design with $\phi = \alpha = 3$, and the nonlinear control design. As expected the high-gain linear

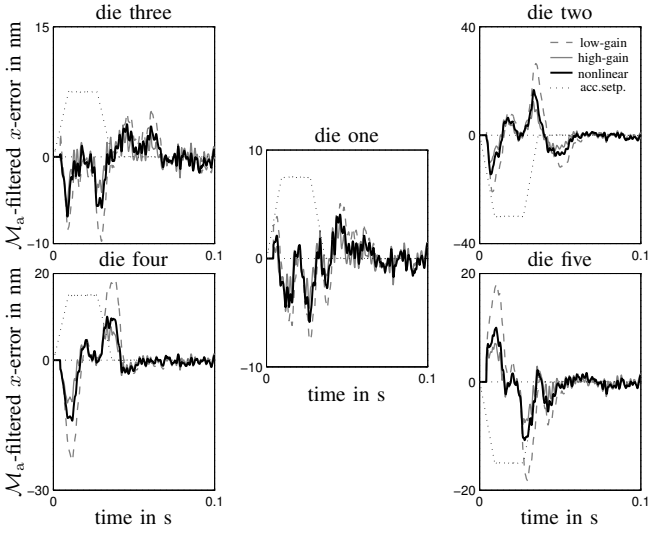

Fig. 10. Time-series simulation of the $\mathcal{M}_{\rm a}$-filtered x-error signals.

and the nonlinear control design perform equally good in terms of keeping the error responses induced by the acceleration set-points (dotted curves denoted by acc.setp.) small. This is due to the extra low-frequency disturbance rejection properties. Contrarily, the low-gain linear control design shows a significantly larger error response for the considered wafer locations and, therefore, associates with less favorable low-frequency disturbance suppression properties.

The advantages of the nonlinear control design come to the fore the clearest in Fig.11. In terms of moving

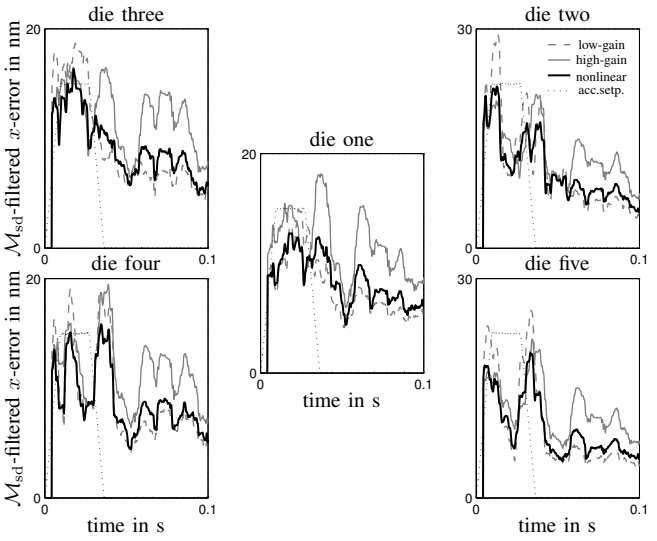

Fig. 11. Time-series simulation of the $\mathcal{M}_{\rm sd}$-filtered x-error signals.

standard deviation error responses, this figure shows that the nonlinear control design combines the favorable disturbance rejection properties of Fig.10 with a small noise response. More specifically, during the acceleration phases prior to scanning, the nonlinear responses show most resemblance with the (small-amplitude) high-gain responses whose are preferable to the (large-amplitude) low-gain responses. During scanning, however, both the low-gain and nonlinear control design show the smallest noise response, the kind of noise response inaccessible to the high-gain control design. It is therefore concluded that the nonlinear control design combines the best of both low- and high-gain linear control designs in achieving improved wafer scanning performance in view of the considered position-dependent behavior.

V. Conclusions

A nonlinear observer-based control design is presented which combines a high-gain (and low-frequency) disturbance rejection with a low-gain (but high-frequency) noise response. The observer is characterized by a low-pass filter with varying cut-off frequency. Stability is guaranteed in the context of the circle criterion whereas performance is shown to be positively influenced by the usage of a variable gain observer. With a validated simulation model, the nonlinear control design shows improved performance for five considered wafer locations and thereby provides an effective means to deal with position-dependent behavior along the wafer surface. At each location, the responses show improved disturbance suppression but with a superior noise response. This shows the effectiveness of the variable gain observer and supports the idea of nonlinear control for linear systems [17] as a means to improve upon servo performances under varying expression of plant dynamics and system disturbances.

References

[1] Baek J-S, Chung CC, and Tomizuka M. (2006) Anti-shock controller design for optical disk drive systems with a nonlinear controller. In Proceedings of the American Control Conference, Minneapolis, Minnesota, USA:1982-1989.

[2] Fatikow S, Wich T, Hülsen H, Sievers T, and Jähnisch M. (2007) Microrobot system for automatic nanohandling inside a scanning electron microscope. IEEE/ASME Transactions on Mechatronics, 12(3):244-252.

[3] Mishra S, Coaplen J, and Tomizuka M. (2007) Precision positioning of wafer scanners; segmented iterative learning control for nonrepetitive disturbances. IEEE Control Systems Magazine, August:20-25.

[4] Al-Sweiti Y, and Söffker D. (2007) Modeling and control of an elastic ship-mounted crane using variable gain model-based controller. Journal of Vibration and Control, 13(5):657-685.

[5] Armstrong BSR, Gutierrez JA, Wade BA, and Joseph R. (2006) Stability of phase-based gain modulation with designer-chosen switch functions. International Journal of Robotics Research, 25:781-796.

[6] Tahboub KA. (2005) Active nonlinear vehicle-suspension variable-gain control, In Proceedings of the Conference on Control and Automation, Limassol, Cyprus:569-574.

[7] Arcak M, and Kokotović P. (1999) Nonlinear observers: a circle criterion design, In Proceedings of the Conference on Decision and Control, Phoenix, Arizona, USA:4872-4876.

[8] Arcak M. (2005) Certainty-equivalence output-feedback design with circle-criterion observers. IEEE Transactions on Automatic Control, 50(6):905-909.

[9] Ibrir S. (2007) Circle-criterion observers for dynamical systems with positive and non-positive slope nonlinearities, In Proceedings of the American Control Conference, New York City, USA:260-265.

[10] Rahiman W, Li B, Wu B, and Ding Z. (2007) Circle criterion based nonlinear observer design for leak detection in pipelines, In Proceedings of the Conference on Control and Automation, Guangzhou, China:2993-2998.

[11] Tsiotras P, and Arcak M. (2005) Low-bias control of AMB subject to voltage saturation: state-feedback and observer designs. IEEE Transactions on Control Systems Technology, 13(2):262-273.

[12] Johansson R, Robertsson A, and Shitiaev A. (2004) Observer-based strict positive real (SPR) switching output feedback control, In Proceedings of the Conference on Decision and Control, Atlantis, Paradise Island, Bahamas:2811-2816.

[13] Gao Z, Huang Y, and Han J. (2001) An alternative paradigm for control system design, In Proceedings of the Conference on Decision and Control, Orlando, Florida, USA:4578-4585.

[14] Heertjes MF, and Steinbuch M. (2008) Circle criterion in linear control design. In Proceedings of the American Control Conference, Seattle, Washington, USA: 3176-3181.

[15] Yakubovich VA, Leonov GA, and Gelig AKh. (2004) Stability of stationary sets in control systems with discontinuous nonlinearities. World Scientific, Singapore.

[16] Bode CA, Ko BS, and Edgar TF. (2004) Run-to-run control and performance monitoring of overlay in semiconductor manufacturing. Control Engineering Practice, 12:893-900.

[17] Aangenent WHTM, Van de Molengraft MJG, and Steinbuch M. (2007) Time-domain performance based nonlinear state feedback control of constrained linear systems. In Proceedings of the Conference on Control Applications, Singapore: 1297-1302.